Computers & Geosciences 199 (2025) 105917

Contents lists available at ScienceDirect

Computers and Geosciences

journal homepage: www.elsevier.com/locate/cageo

Quantitative bed-type classification for a global comparison of deep-water sedimentary systems

Soma Budai [a,b,*], Luca Colombera [a], Adam McArthur [b], Marco Patacci [c]

[a] Dipartimento di Scienze della Terra e dell'Ambiente, Università degli Studi di Pavia, Via Ferrata 1, 27100, Pavia, Italy
[b] Turbidites Research Group, School of Earth and Environment, University of Leeds, Leeds, LS2 9JT, United Kingdom
[c] Dipartimento di Medicina Clinica, Sanità Publica, Scienze della Vita e dell'Ambiente, Università degli Studi dell'Aquila, Piazzale Salvatore Tommasi 1, 67010, L'Aquila, Italy

ARTICLE INFO

Keywords:
Deep-water deposits
Sedimentary bed
Turbidites
Facies
Training dataset
Quantitative sedimentology

ABSTRACT

Characterisation of deep-water successions is often undertaken at the scale of sedimentary beds. However, different studies often apply alternative bed-type classification schemes, rendering the quantitative comparison of bed properties of different deep-water systems difficult. In this study a quantitative approach to the development of a universal deep-water bed-type classification scheme is proposed based on the synthesis of a large sedimentological dataset, containing >32,000 deep-water facies and >10,000 beds accumulated in 27 turbidite-dominated systems. The classification scheme is applicable to discriminate and categorise lithological (sand, gravel) layers and is based on: (i) the proportion of, gravel, sand, sandy-mud and muddy-sand in the bed, (ii) the presence and nature of vertical sharp grain-size changes, and (iii) the presence and thickness ratio of laminated sedimentary facies. Comparing the bedding properties of channel-fills, terminal deposits (e.g. lobes or sheets) and levees showed that the three architectural-element types are characterised by differences in bed frequency and thickness, overlying mudstone proportions, vertical bed thickness trends, mud thickness and sand-gravel fraction values. Building on these recognised statistical differences an algorithm was developed that is capable of generating, in a stochastic manner, geologically realistic synthetic sedimentary logs depicting deep-water terminal-deposit, channel-fill and levee elements. The one-dimensional facies modelling is governed by a series of input parameters, including total number of beds, sand-gravel thickness, and sand-gravel fraction. The approach can be tailored to produce synthetic logs for specified types of depositional systems (e.g., categorised according to dominant grain size of deposits, age of deposition and global climate (icehouse vs. greenhouse conditions)). A large number of synthetic sedimentary logs can be generated, which can be utilised as training datasets in machine learning algorithms developed to aid subsurface interpretations of clastic sedimentary successions.

1. Introduction

In deep-water clastic successions, beds are commonly defined as the preserved record of individual sediment gravity-flow events (Bouma, 1962; Lowe, 1982). Thus, their thickness, internal structure and vertical trends depend on the characteristics of their formative flow, with variations within a bed expressed in vertically stacked facies characterised by differences in grain-size and sedimentary structures (Mutti, 1992; Talling et al., 2012). The formative flow characteristics are themselves dependent on multiple controlling factors, such as climate, sea level, basin topography, confinement, and substrate characteristics, among others (Mutti and Normark, 1987, 1991), and tend to vary in time and longitudinally along the flow itself (Mulder and Alexander, 2001). Sedimentary beds are the basic building blocks of deep-water clastic successions, as sets of bed accrete to build architectural elements including lobe, channel-fill and levee elements (Lowe, 1982; Mutti and Normark, 1987; Mutti, 1992; Pickering et al., 1995; Pickering and Hilton, 1998). The deposits of these elements may form significant reservoirs and aquifers (e.g. Bell et al., 2018; De Ruig and Hubbard, 2006; McKie et al., 2015) and are characterised by distinct facies and bed-thickness properties (e.g., Deptuck et al., 2008; Felletti and Bersezio, 2010; Fryer and Jobe, 2019; Jobe et al., 2024; Mutti and Normark, 1987; Prélat et al., 2009).

Sedimentological studies of deep-water successions often propose

* Corresponding author. University of Pavia, Via Ferrata 1, 27100, Pavia, Italy.
E-mail address: soma.budai@unipv.it (S. Budai).

https://doi.org/10.1016/j.cageo.2025.105917
Received 14 November 2024; Received in revised form 24 January 2025; Accepted 10 March 2025
Available online 10 March 2025

bespoke classification schemes for bed types, typically with emphasis on classes that are interpretable in terms of flow processes (e.g. Cronin and Jones, 2018; Łapcik, 2024). However, as different studies apply different classification schemes for facies types or bed types, qualitative and quantitative comparisons of different deep-marine successions are hindered. Previously proposed general bed-type classification schemes (e.g. Ghibaudo, 1992; Pickering et al., 1986) are usually meant to be used for detailed field-based sedimentological studies, and are generally too complex and inflexible to be used for comparing data originating from different sources. Most previous studies undertaking comparisons of the bedding properties of deep-water systems or different elements were restricted to the analysis of bed thickness or shape (e.g., tabularity), considering the lateral and vertical variability of these properties (e.g., Felletti, 2002; Felletti and Bersezio, 2010; Fryer and Jobe, 2019; Jobe et al., 2024; Pantopoulos et al., 2018; Sylvester, 2007; Tőkés and Patacci, 2018). Studies focusing on the comparison of bed-type properties usually focused on differences between local datasets from the same turbidite system (e.g., Felletti, 2004). Such limitations affecting earlier studies reflect the lack of an approach that could be utilised to compare a large number of deep-water systems effectively. A generalised classification approach based on objectively recognised sedimentary features of beds produced by sediment gravity flows would enable a quantitative comparison between different depositional systems that formed under different conditions, throughout geological time.

The aim of this study is therefore to propose a deep-water bed-type classification scheme based on simple and objective sedimentological criteria, which could be applied to the quantitative analysis of the deposits of multiple deep-water sedimentary systems. Using a database-driven approach, this was achieved through the following objectives: (i) A synthesis of data from twenty-seven turbidite-dominated depositional systems, including examples from the Neoproterozoic to the Holocene, including a total of more than 32,000 facies and more than 10,000 beds; (ii) The development of a script, coded in R, for the classification of sedimentary beds stored in a large sedimentological database – the Deep-Marine Architecture Knowledge Store (DMAKS; Cullis et al., 2019) – into objectively defined types based on a selected set of facies properties; (iii) A demonstration of how this bed-type classification can be used to quantify differences in bedding properties (e.g. bed-type frequency, thickness etc.) of selected types of deep-water architectural elements: terminal-deposit (lobe or sheet), channel-fill and levee elements; (iv) The creation of a stochastic algorithm, coded in R, that can be utilised to create synthetic 1D sedimentary logs of architectural elements based on geological-analogue data on their bedding architecture, which could serve as training datasets for machine learning algorithms aiming to automate subsurface sedimentological interpretations.

2. Database

A novel database-driven approach has been developed to categorise

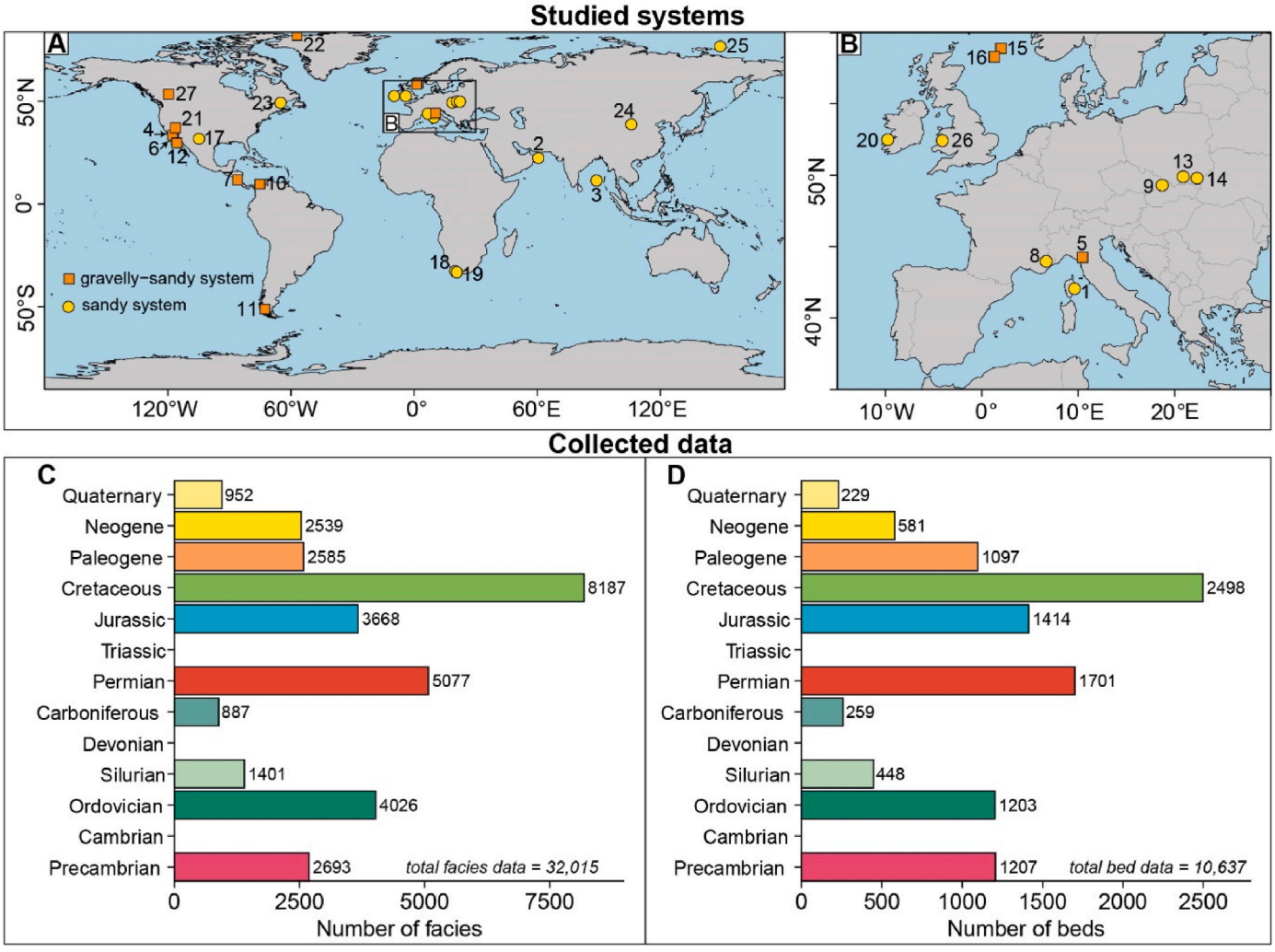

Fig. 1. (A,B) Geographical position of the studied deep-water systems; the numbers labelled on the map refer to the identifiers of each case study, as reported in Table 1. Bar charts of the numbers of studied facies units (C) and beds (D) charted based on their age.

deep-water sedimentary bed types based on quantitative data on their lithological (facies) characteristics. The data employed for this purpose have been compiled from 27 turbidite-dominated depositional systems from 41 published sources (Fig. 1; 2A, Table 1). The data are stored in the DMAKS relational database, which contains qualitative and quantitative data on the sedimentological characteristics of deep-water marine and lacustrine depositional systems, and on geological attributes of their host basin and depositional setting (Cullis et al., 2019, Fig. 2). Sedimentary architectures are captured in the form of sedimentary units at multiple scales: architectural elements of different hierarchies and facies units. Data that are relevant for this study were originally collected from both outcrop and subsurface core studies, describing both modern and ancient deep-water clastic depositional systems (Fig. 1 and Table 1).

In DMAKS, a depositional system is defined to encompass the whole sediment-transport and deposition pathway in a clastic deep-water setting. In a classic shelf-slope-basin-floor profile, this pathway extends from the shelf-slope break to the most distal areas reached by gravity flows (Mutti, 1992; Normark, 1970). For each depositional system, the recorded attributes include their location, age, lithostratigraphy, dimensions, palaeo-latitude, continental-margin type and tectonic setting at the time of deposition. The dimensions, age, shape,

Table 1
Deep-water systems recorded in DMAKS and used in this study.

ID	System	Latitude	Longitude	Basin	Period	Grain size	N facies	N beds	Reference
1	Golo Turbidite System	42.05	9.61	Golo Basin	Quaternary	sandy system	587	82	Pichevin et al. (2003); Gervais et al. (2006); Deptuck et al. (2008)
2	Al Batha Turbidite System	22.4	60.59	Gulf of Oman Basin	Quaternary	sandy system	39	3	Bourget et al. (2010)
3	Bengal Fan	11.45	88.85	Rakhine Basin	Quaternary	sandy system	326	144	Yang and Kim (2014)
4	Capistrano Formation	33.52	−117.6	Capistrano Embayment	Neogene	gravelly-sand system	797	326	Campion et al. (2007); Li et al. (2016)
5	Torre degli Amorotti turbidite system	44.25	10.46	Cervarola Basin	Neogene	gravelly-sand system	1742	255	Tinterri and Piazza, 2019
6	Black's Beach	32.89	−117.25	San Diego Basin	Paleogene	gravelly-sand system	223	84	Stright et al. (2014)
7	Brito Formation Turbidite System	11.75	−86	Sandino Basin (during the Brito Fm)	Paleogene	gravelly-sand system	619	153	Brandes et al. (2007); Struss et al. (2007)
8	Grès d'Annot Formation	43.96	6.68	Alpine Foreland Basin	Paleogene	sandy system	764	407	Brunt (2003)
9	Raca unit turbidite system	49.31	18.72	Magura basin	Paleogene	sandy system	540	246	Staňová et al., 2009
10	San Jacinto turbidite system	9.75	−75.1	Caribbean basin	Paleogene	gravelly-sand system	439	207	Celis et al. (2024)
11	Cerro Toro Deep-Water System	−51.08	−72.68	Magallanes Basin (during the Cerro Toro)	Cretaceous	gravelly-sand system	1479	73	Barton et al., 2007a
12	San Fernando Turbidite System	29.75	−115.6	Rosario Embayment (during the Rosario Fm)	Cretaceous	gravelly-sand system	4442	1848	Dykstra and Kneller (2007); Kane et al. (2007), 2009; Callow et al. (2013)
13	Ropianka turbidite system (West)	49.9	20.9	Skole basin (West)	Cretaceous	sandy system	1155	223	Łapcik (2024)
14	Ropianka turbidite system (East)	49.79	22.33	Skole basin (East)	Cretaceous	sandy system	1111	354	Łapcik (2017)
15	Draupne Formation turbidite system	58.9	2	South Viking Graben	Jurassic	gravelly-sand system	371	116	Jackson et al. (2011)
16	Thelma Field turbidite system	58.3	1.3	South Viking Graben	Jurassic	gravelly-sand system	3297	1298	Cronin and Jones (2018)
17	Brushy Canyon	31.76	−104.78	Delaware Basin (during the Brushy Canyon)	Permian	sandy system	619	168	O'Byrne et al. (2007); Pyles et al. (2010)
18	Tanqua Karoo	−32.67	20	Tanqua Karoo Subbasin (during the Skoorsteenberg Fm)	Permian	sandy system	987	330	Hofstra et al. (2015); Kane et al. (2017)
19	Laingsburg Karoo Turbidite System	−33.19	20.86	Laingsburg depocentre	Permian	sandy system	3471	1203	Figueiredo et al. (2010); Hofstra et al. (2015); Morris et al., 2014a, 2014b
20	Ross Sandstone Turbidite System	52.5	−9.75	Shannon Basin	Carboniferous	sandy system	559	205	Pyles (2007a), 2007b
21	Antler foredeep turbidite system	37.1	−116.19	Antler foreland Basin	Carboniferous	gravelly-sand system	328	54	Trexler and Cashman (1997)
22	Peary Land Group turbidite system	82	−57	Franklinian Basin	Silurian	gravelly-sand system	1401	448	Larsen and Escher (1991)
23	Cloridorme turbidite system	49.22	−65.03	Taconic foreland basin (during Cloridorme Formation)	Ordovician	sandy system	650	219	Ningthoujam et al. (2022)
24	Yingtaogou turbidite system	38.77	105.81	Western margin of the North China Craton	Ordovician	sandy system	490	24	Wang et al. (2021)
25	Bennett Island turbidite system	76.67	149.17	Bennett Basin	Ordovician	sandy system	1369	752	Danukalova et al., 2020
26	Aberystwyth Grits	52.43	−4.08	Southern Welsh basin	Ordovician	sandy system	1517	208	Baker and Baas (2020); Baas et al. (2021)
27	Isaac Formation	53.47	−119.62	Not Specified	Precambrian	gravelly-sand system	2693	1207	Navarro et al. (2007); Barton et al., (2007a, 2007b); Ningthoujam et al. (2022)

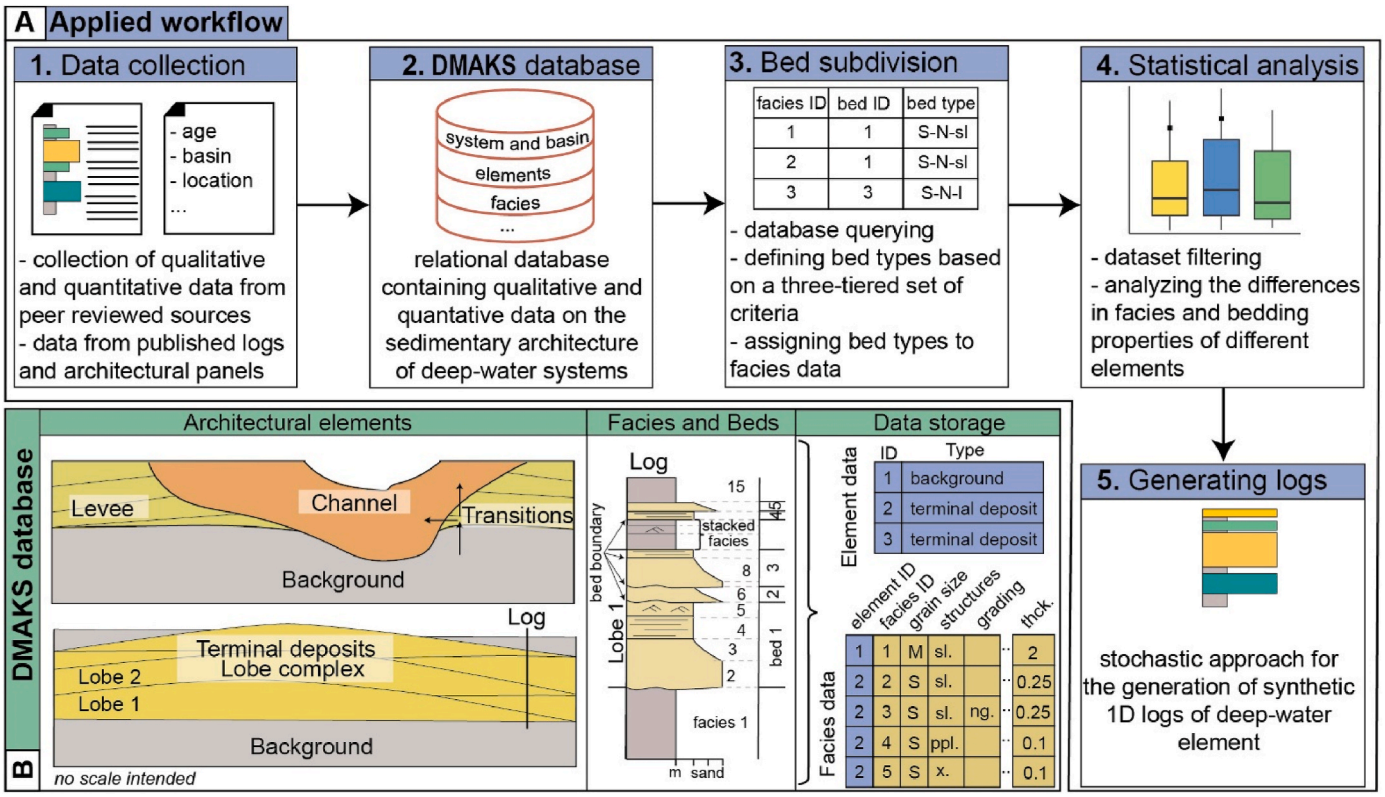

Fig. 2. (A) Applied workflow for the definition of deep-water bed types. Data collected from different published sourced on elements and facies of deep-water systems are stored in the DMAKS database. An R script assigns a bed type to every stored bed based on a three-tiered set of criteria (Fig. 3). Then, bedding properties are analysed to determine differences between channel-fill, levee and terminal deposits. These statistical differences are utilised to inform a script that generates stochastic synthetic 1D sedimentary logs of the above architectural elements. (B) Stored attributes of the DMAKS database; architectural sketch and facies log are not to scale.

and topographic characteristics of sedimentary basins, and of topographic depocentres that may have existed through the lifetime of a basin, are also recorded.

Data on architectural elements were collected from 2D and pseudo-3D outcrop or well correlation panels, and 1D sedimentary logs. In DMAKS, architectural elements are defined as sedimentary bodies or geomorphic elements representing a specific deep-water sub-environment, characterised by a distinct architectural or geomorphological expression, formed by a specific set of processes (Cullis et al., 2019). Architectural elements are classified according to different classification schemes (e.g., type and shape); among these schemes, a classification is operated whereby elements are categorised into terminal deposits (i.e., lobesor sheets), channel-fill and levee elements, among other classes (Fig. 2B). A three-tiered data quality index is assigned (attributing ordinal classes 'A', 'B' or 'C' in decreasing order) to rank the classification of each element in terms of underlying data quality and sensibility of interpretations. This study focuses on the sedimentary architecture of these three element types, in view of their common occurrence in deep-water successions. Architectural elements can exist over multiple hierarchies, which are digitised in DMAKS; for example, hierarchical relationships between terminal deposits (e.g., 'lobes', 'lobe complexes') or channel-fill elements (e.g., 'storeys', 'complexes') at different scales are captured via a record of the containment of lower-scale elements in larger-scale elements (parent-child relationships).

Architectural elements are made of facies units. Individual facies units represent basic lithological units distinguished on the basis of changes in sediment texture, sedimentary structure and/or presence of intervening bounding surfaces (Fig. 2B). The database hosts facies data originated from outcrops, cores or from wireline logs and can be filtered based on data type. Data on facies units analysed in this study are collected from published, interpreted, facies-based, 1D sedimentary logs measured in either outcrops or on cores. Recorded properties of each facies unit includes their grain size based on Folk's textural classes (Folk, 1980). These categories include mud, sand and gravel classes and mixtures of these, such as gravelly sand, sandy mud, muddy sand, etc. Other recorded attributes include the type of basal boundary of each facies (e.g., erosional, gradational) and a Boolean attribute indicating whether the boundary has been interpreted and indicated as an event-bed boundary (in the original log of the source dataset). For each facies unit, additional information is included in attributes describing sand grain size, presence and type of sedimentary structures and grading among others.

Spatial relationships between different sedimentary units of the same rank (i.e., between architectural elements and between facies units) are also recorded, in the form of transitions along the vertical, downdip and strike directions (Fig. 2). When known, the lateral extent and distality of facies units within their parent architectural elements are also recorded using positional classifiers for the lateral (from the axis/core to the margin/fringe) and dip (proximal, medial and distal) directions.

Quantitative data on the geometry of elements and facies (thickness, width and length) stored in DMAKS were extracted from 2D panels or sedimentary logs using image-analysis software (ImageJ) or directly from the text of the published data source. Vertical and lateral dimensions of units stored in the database can be classified as 'true', 'apparent', 'partial' and 'unlimited' (Geehan and Underwood, 1993). The 'true maximum' thickness, length and width of architectural elements is only recorded where some pseudo-3D reconstruction of the element geometry is possible; 1D datasets like sedimentary logs only yield 'apparent' thickness data for both elements and facies when both the underlying and overlying units are observed. If either the base or the top of the unit is not observed, the thickness value is classified as

'partial', whereas it is classified as 'unlimited' when neither base nor top are observed. In the analyses of vertical facies trends and facies proportion, only elements whose vertical extent was fully observed (true or apparent) were considered.

The dataset analysed in this study includes data on 32,015 deep-water facies units (including mud, sand and gravel facies) belonging to 438 architectural elements (Fig. 1).

3. Bed type analysis

3.1. Defining bed types

In the DMAKS database, different sedimentary facies that were laid down by the same depositional event, either a single- or multipulse flow event, can be grouped and linked to individual beds. The attribution of facies units to event beds is done on the basis of interpretations provided by the authors of the original sedimentological study from which the data are derived (e.g., based on the presence of bed boundary surfaces on the sedimentary log). Many literature studies do not attempt the discrimination of mud-rich facies representing mudstone caps, deposited from the diluted tails of flow events, from hemipelagic mud, settled from suspension between flow events. Due to a lack in consistency in discriminating these two types of mud-prone deposits, an approach is proposed in this study for the classification of lithological beds, consisting of the sandstone- and/or gravel-prone portions of event beds (Fig. 2B). In this study 19,888 deep-water facies units containing sand and/or gravel fraction were considered to create a general bed-type scheme useable to compare data from different sources and to carry out statistical analysis in a consistent way (Figs. 1, 3 and 4).

A script called DW-BC (Deep-Water Bed Classifier) was created in R (version 4.4.0) (R Core Team (2021) that draws data from the DMAKS database through SQL queries and sequentially applies a three-tiered set of criteria to the vertical facies sequence of each stored bed to classify them into pre-defined bed types (Fig. 2A and 3). In the R script, the 'RMariaDB' (Müller et al., 2024) package was used to query the DMAKS database, the package 'dplyr' (Wickham et al., 2023) was used to manipulate the data, while 'ggplot2' (Wickham, 2016) was used to generate plots.

As a first step, based on data records of the presence of bed bounding surfaces between each vertically superimposed facies, the script groups vertically stacked facies units into individual beds with an assigned bed identification number (Fig. 2B). This initial step is followed by the calculation of bedding properties based on: (i) lithology (sand/gravel ratio and presence of sand/mud mixtures), (ii) presence of sharp grain-size changes (including changes in sand grain size across sandy facies units), (iii) presence and proportion of any kind of laminations or sub-bed scale stratification (e.g., planar parallel lamination, ripple cross-lamination) (Fig. 3). Finally, each bed is classified and associated with an alphabetic code based on these three key features of its facies units (Fig. 3). The approach was devised to ensure that (i) the created bed-type scheme can be applied universally (Fig. 4), and that (ii) a classification can be made consistently across sources with heterogeneous and partial datasets (e.g., in cases where only grain-size descriptions are reported and no data on sedimentary structures are available). This latter goal was achieved by the sequential application of bedding properties to each bed (Fig. 3). The dataset contains 10,637 sandstone and gravel beds where all three examined attributes were observable. Currently, the proposed bed-type classification is only based on the above three attributes, as relevant quantitative data can be readily extracted from published sedimentary logs. Attributes such as the presence and style of grading within distinct beds, oversized-clast content or post-depositional facies attributes (e.g., bioturbation, dewatering structures) can be incorporated in the classification approach in the future. Relationships with underlying and overlying facies and thickness data were also not considered in the classification approach.

The first criterion applied for bed classification pertains to the lithology. Based on the relative proportion of gravel and sand in the beds (obtained as a thickness ratio and reported as percentage), sand-rich and gravel-rich end-member beds are assigned where sandy and gravelly facies are exclusively present, respectively (Fig. 3). Between these two end-members, two intermediate types are defined: sandy-gravel (dominated by gravel) and gravelly-sand (dominated by sand) beds, based on a threshold of 50 % gravel-sand thickness proportion. Beds that contain at least one facies of muddy-sand or sandy-mud lithology were classified into a separate group called: muddy-sandy beds. These five bed categories are denoted by a code as follows: G (gravel), S (sand), sG (sandy gravel), gS (gravelly sand), MS (muddy sandy) (Fig. 3).

The second classification criterion is based on the presence of sharp facies-unit transitions within beds and grain-size changes associated with them, including changes in sand grain size across sandy facies. Numerical values were assigned to each facies within beds based on the combination of their facies and sand grain-sizes in a fining order, from gravel to sandy mud with very fine sand fraction. For each bed, the script calculates the difference in these assigned values between each facies and the overlying one. Then the minimum and maximum of these differences for each bed are determined; these two numbers are referred to as 'grain-size trend score'. In cases where these values are both equal to zero or where the bed is composed of only one facies, then the bed is

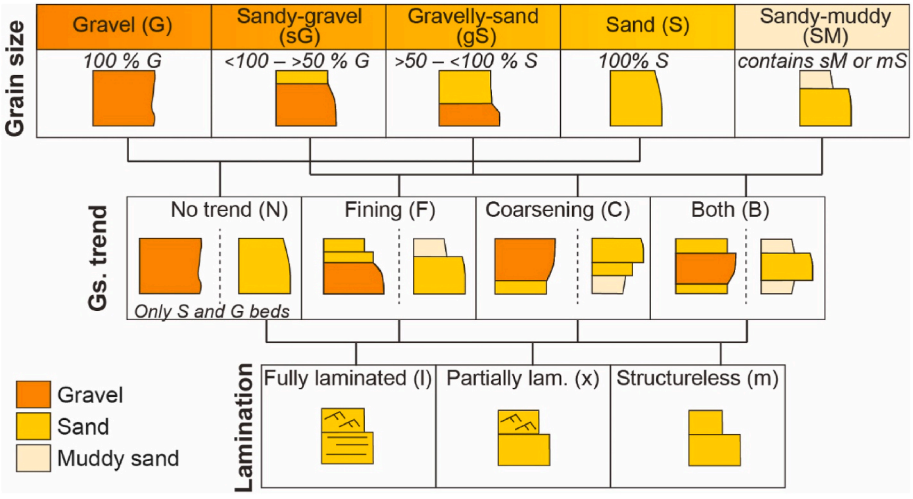

Fig. 3. Features used to classify deep-water bed types: gravel, sand and sandy mud/muddy sand proportion; presence and type of sharp grain-size changes through the profile; presence and proportion of laminations.

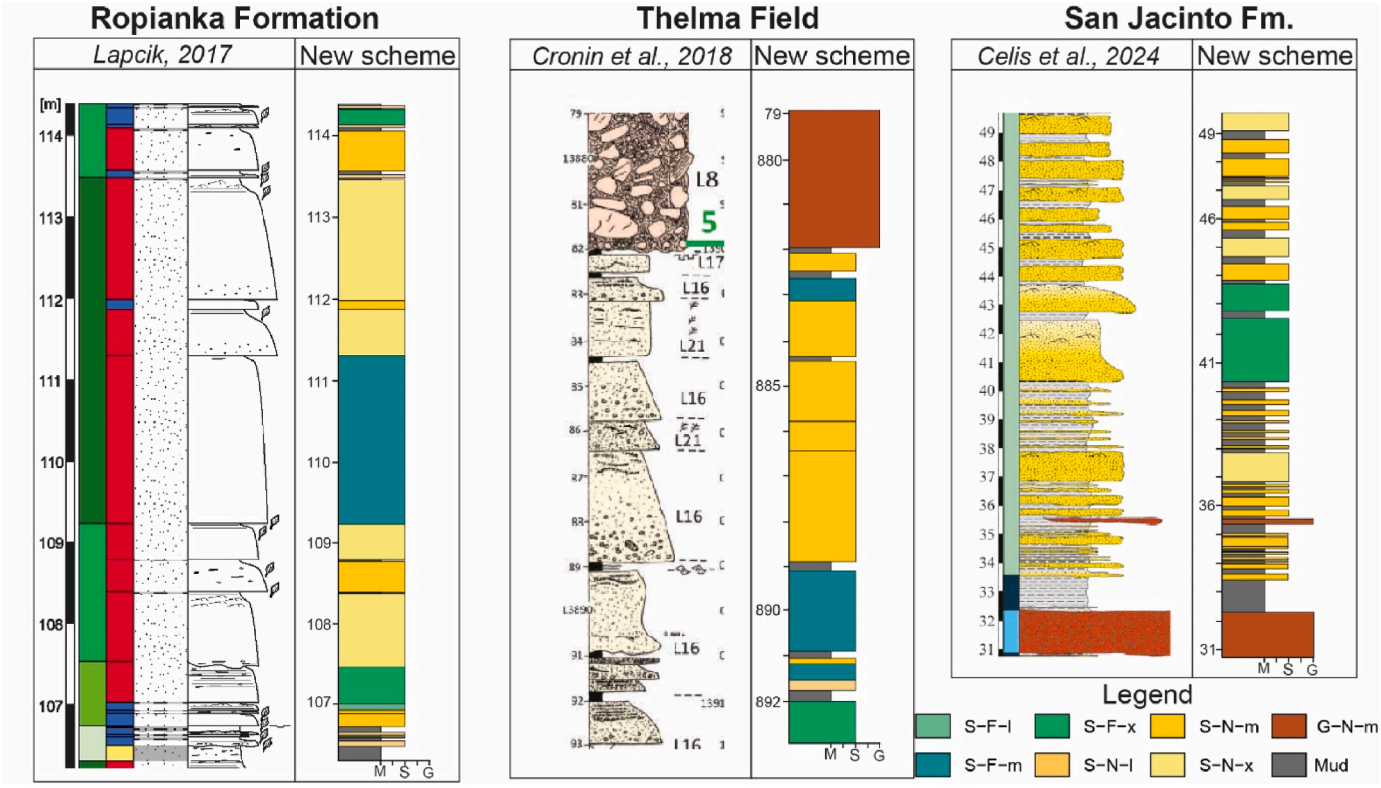

Fig. 4. Examples from the collected dataset. The figure shows sedimentary logs drawn by different authors and the type of the illustrated beds based on the proposed global bed-type scheme.

characterised as showing no vertical trend (category N). If the maximum value of the calculated differences is negative, then a fining-upward trend (category F) is assigned to the bed; if the minimum value is positive then the bed is classified as coarsening upward (category C). If both coarsening and fining trends are observed among the facies units composing the bed at hand (i.e., if the minimum value is negative and the maximum value is positive) without any preferential ordering, then the bed falls into the 'B' category, which indicates the presence of both grain-size trends over the vertical profile of the bed.

This classification is only operated by considering sharp transitions, disregarding grain-size trends within portions of beds that exhibit grain-size grading (normal or inverse grading). In the case of facies that exhibit grading, the grain-size trend score is calculated from the grain size of the basal and topmost facies of the gradational part and its relation to the underlying and overlying facies respectively. This means that purely gradational beds would fall into the 'N' category, which flags the absence of sharp trends.

The third and last considered bed characteristic is the presence and proportion of any kind of lamination in sandy and gravelly facies of the beds. The cumulative thickness of the laminated or stratified portion (e.g., planar-parallel lamination, ripple cross-lamination, mesoform-scale cross-stratification and wavy cross-stratification) of each bed was compared to the total bed thickness. Based on these thickness ratios, three categories were established: beds that lack any kind of lamination or stratification (m), beds that are fully made of laminated or stratified facies (l) and beds that are only in part made of laminated or stratified facies (x).

3.2. Bedding properties of deep-water architectural elements

A statistical analysis (Fig. 2A) was carried out to reveal differences in the bed types, bed vertical transitions and bed thickness of terminal deposit, channel-fill, and levee elements. In this study, these three architectural element types were selected for analysis as they represent fundamental building blocks of deep-water successions. Furthermore, specific focus is placed on results of analysis carried out on DMAKS deep-water depositional systems whose facies units yield a sand fraction, relative to the cumulative sand and gravel content, higher than 95 %; these sedimentary successions are termed 'sandy systems' hereafter. Out of the 27 studied systems, 15 fall into this category; sandy systems contain 4568 of the total 10,637 beds where all three bedding attributes (Fig. 3) were characterised.

Bed-type frequencies were calculated based on the number of observations of a specific bed type divided by the total number of beds in a specific subset of the dataset; these frequencies were reported as percentages. The studied sand-dominated subset of the total dataset is dominated by the presence of 'sand' beds (Fig. 5). Nearly 60 % of the considered beds belong to the structureless sand bed category (S-N-m), while the second most common bed type, purely laminated sand beds (S-N-l), only represent 15 % of the total bed count (Fig. 5). Analysing the bed-type frequencies of different architectural elements showed that the 'structureless sand bed' (S-N-m) class was the most frequent bed type in the studied terminal deposits and channel-fills. Aside from these two bed types, partially laminated (S-N-x) and partially laminated fining-upward sand beds (S-F-x) are also common. On the other hand, levee deposits were dominated by purely laminated beds (S-N-l) (Fig. 6A). Beds with sandy-mud or muddy-sand facies (SM category) represent only a small portion of the analysed dataset and are described in 8 of the 27 studied deep-water systems. Only beds containing either sandy-mud or muddy-sand facies (SM-N-m) and beds where these facies are arranged into a fining-upward trend (SM-F-m) reach frequencies above 1 % in terms of bed counts. Furthermore, this bed type is only observed in terminal deposits, and is instead absent in the examined channel-fill and levee deposits (Fig. 6A).

In the analysis of vertical transitions, each sandstone/gravelly bed can be overlain by another sandstone/gravelly bed or by a mudstone layer. The probability of a bed being overlain by a mudstone layer is referred to as "overlying mudstone probability". These values were

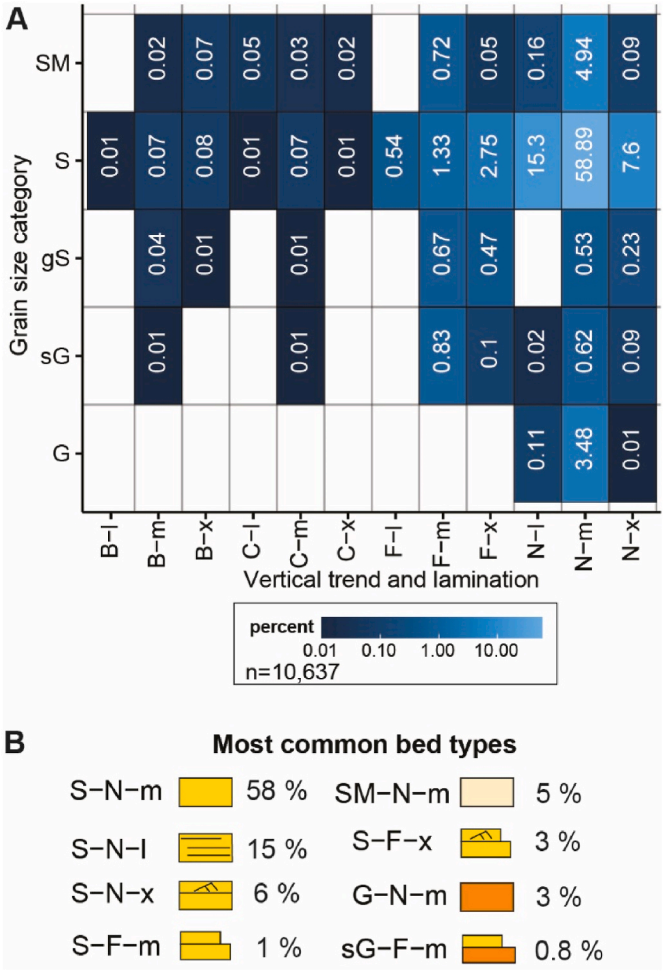

Fig. 5. (A) Heathmap showing the frequency (based on number) of different bed-types on the total dataset. (B) Example depiction and frequency of most common bed types.

calculated as the percentage of transitions with a bed top being overlain by a mudstone layer relative to the total number of observed vertical transitions for each bed top (Fig. 6B). In general, the studied beds of channel-fill elements are significantly less likely to be overlain by muddy facies (22 %) compared to beds of terminal deposits (57 %) and levee elements (90 %) (Fig. 6B). In other words, sand or gravel bed amalgamation is higher on average in channelised deposits. In channel-fill elements, the highest overlying mudstone probability does not exceed 45.3 %, which is observed for fully laminated sand beds (S-N-l); structureless sand beds (S-N-m) are the least likely to be overlain by fine grained sediments (17.2 %). Similarly, for terminal deposits, structureless sand beds are the least likely to be overlain by a muddy interval (42 %), whereas all other observed bed types are expected to be overlain by fine-grained sediments. Overlying mudstone probabilities reached at least 80 % for all the five bed types seen in levee deposits.

For bed-thickness analysis and comparison, only sedimentary logs capturing sediments at the same vertical resolution (mm to cm) were considered. In the studied sandy deep-water systems, individual beds attained on average higher thickness values in channel-fill elements than in terminal deposits, while levee elements are characterised by much thinner beds on average (Fig. 6C). The mean and median thickness of beds are largest in channel deposits for all bed types except S-N-l. In the case of the studied terminal deposits and channel-fill elements, 'fully laminated' beds are characterised by lower thickness values on average, whereas such beds attain the largest thickness in levee elements (Fig. 6C). Partially laminated sand beds, either with fining-upward trends (S-F-x) or without sharp grain-size changes (S-N-x), tend to be thicker than other bed types in terminal deposits and channel fills.

Aside from bedding properties the stacked-mud thickness of the studied architectural elements was also analysed along with the sand-gravel fraction. The latter was calculated as the ratio between its cumulative sand and gravel thickness and the cumulative thickness of all its facies units for elements with 'apparent' or 'true' thickness records. The differences in the median thickness of muddy intervals of the studied elements do not exceed 0.03 m, whereas the mean thickness value is higher in the case of levee deposits (0.51 m; 0.27 m and 0.24 m for channel-fill elements and terminal deposits; Fig. 6D). The large mean value in mud thickness seen for levee elements reflects the occasional occurrence of m-thick fine-grained intervals. Studied terminal deposits and channel fills are characterised by higher sand-gravel fraction values compared to levee elements (Fig. 6E), and this is reflected in the higher overlying mudstone probability of levee elements (Fig. 6B).

To analyse vertical trends in bed thickness, a 'thickness trend value' was calculated for each segment of sedimentary log intersecting the architectural element of interest. In the analysis of facies and bed-type proportions, thickness and facies transitions, all sedimentary logs were used regardless of the type of thickness observation recorded for the bed-formating facies units. For the analysis of vertical facies trends, only architectural elements whose entire vertical profile was captured by the sedimentary logs (i.e., 'true' and 'apparent' thickness values recorded) were considered. The 'thickness trend value' was calculated as follows: (i) the difference between the thickness of each bed and the thickness of the bed above was computed, considering both beds that are in direct contact, as well as beds separated by mud intercalations; (ii) the total sum of these differences was divided by the sum of the thickness of the beds, to make the different logs comparable. If the calculated value was positive (i.e., if the magnitude and/or number of positive vertical thickness changes outweighs the negative ones), then that specific 1D representation of the element was classified as 'thickening upward'; if instead the value was negative, the element was classed as 'thinning upward'. The studied terminal deposits of sandy systems tend to exhibit thickening-upward trends in sand beds (Fig. 6F). Channel-fill and levee elements are instead characterised by a thinning-upward trend in the majority of cases; this is in agreement with previous studies (e.g., Felletti, 2002; Kane et al., 2007).

4. Application: synthetic sedimentary-log generation

Sedimentological interpretations of borehole cored intervals and of facies logs based on the processing of subsurface wireline well logs can be aided by the use of tools based on artificial intelligence (e.g., Bressan et al., 2020; Halotel et al., 2020; Martin et al., 2021). This approach has also been applied to the interpretation of deep-water architectural elements in subsurface facies data based on geological analogues and quantitative facies models (e.g., Martin et al., 2022). However, these machine learning approaches require training datasets that are coded consistently and contain a vast amount of data. The discussed bed-type scheme and classification method is based on a large dataset that has been compiled by aggregating data from different systems following a common standard; thus, the proposed approach satisfies these two criteria.

The collected and analysed geological-analogue data (Fig. 6) were utilised in an R script for the generation of artificial sedimentary logs, called DW-SLG (Deep-Water Sedimentary Log Generator). DW-SLG incorporates a stochastic algorithm for producing synthetic one-dimensional sedimentary logs illustrating the bedding style of specific deep-water element types (terminal, channel-fill and levee deposits). The bedding properties of synthetic logs generated by the script could serve as features of a training dataset for machine learning algorithms specialising in automated sedimentary-log interpretation.

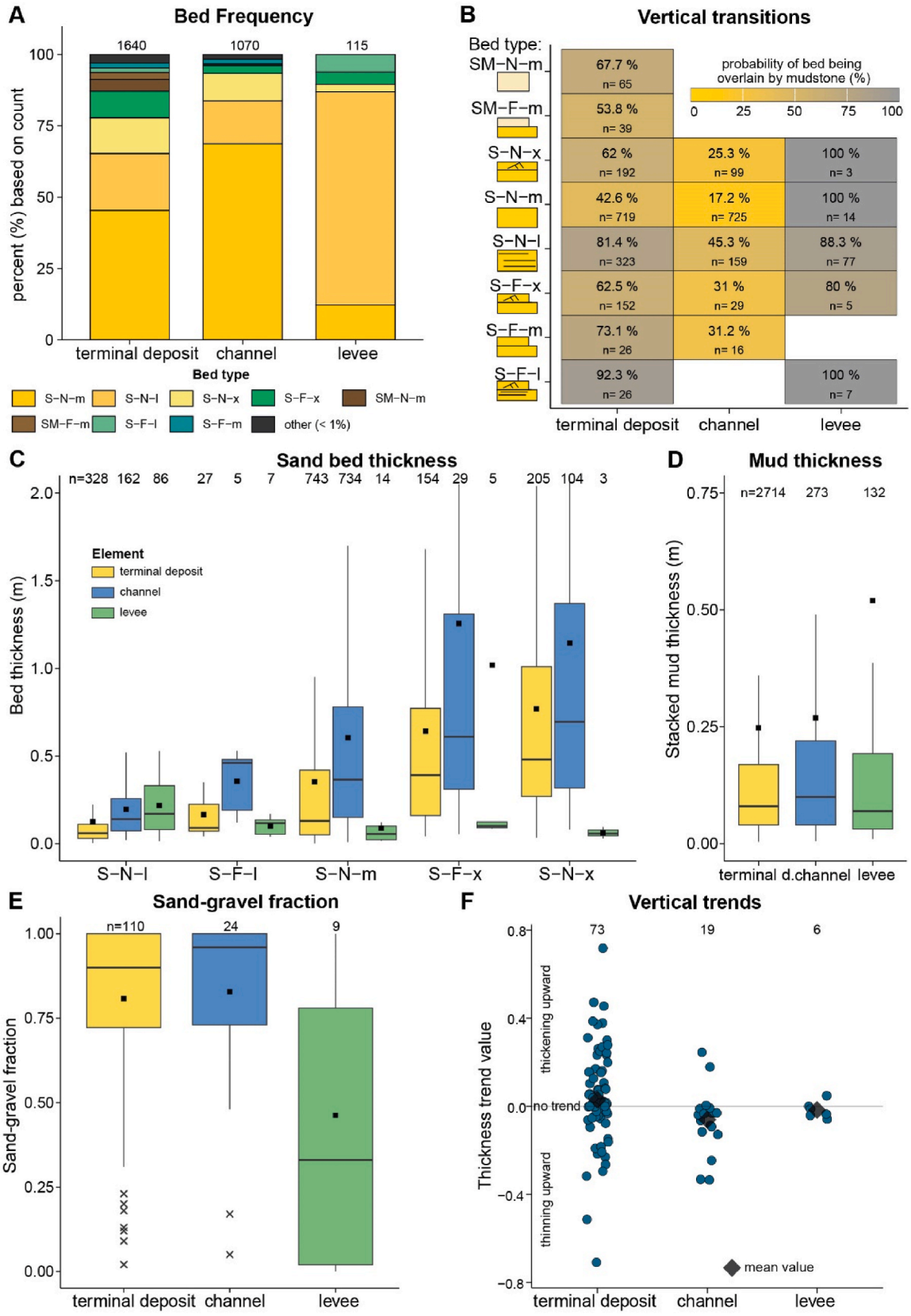

Fig. 6. Plots showing differences in bed properties of channel-fill, levee and terminal deposits of sand-rich deep-water systems: (A) stacked bar chart showing the relative frequency of different bed types; (B) heatmap showing overlying mudstone probability for the most frequent bed types; (C,E) boxplots depicting sandstone bed thickness for the most frequent bed types (C), stacked mud thickness ranges (D) and sand-gravel fraction (E) for different elements (median and mean values indicated in the boxplots); (F) calculated 'thickness trend values' for different elements.

4.1. Sedimentary log modelling process

In the modelling process for the production of synthetic sedimentary logs, the collected dataset on bedding characteristics (Fig. 6) is filtered by a set of input variables (Table 2). These variables include the type of the modelled architectural element along with the climate under which the studied deposits accumulated and their age. Furthermore, specific bed types can be selectively excluded from the modelling process (e.g., exclusion of beds with gravel). This filtered analogues dataset is used by the algorithm to assess the bed-type frequencies and thickness, vertical transitions and thickness trends along with element sand-gravel fraction and mud thickness of the generated logs using a stochastic approach.

Another set of input variables govern the facies characteristics of the output synthetic logs for the chosen element type. These variables include the cumulative sand-gravel thickness, number of beds and sand-gravel fraction, and are described below in detail (Table 2). The script can generate any number of realisations (artificial facies logs) in a single run. Random number generators in the script are governed by seed numbers, to ensure reproducibility. For the batch generation of multiple logs a number of seeds needs to be specified.

As a first step in the modelling process, the algorithm proceeds to estimate the number of occurrences of each bed type in one of two ways, to be chosen by the user. As a first option, the number of bed-type occurrences can be determined based on the random sampling of data on bed frequencies and the desired number of beds to be reproduced in the log (Fig. 7). The total number of beds can be specified as a single value or as a range from which the script draws a value at random (this is done separately for each iteration when multiple logs are generated at once). As a default the dataframe containing the modelled beds is populated using a random number generator that samples a probability density function (PDF) of bed type proportions (e.g., Fig. 6A). As an alternative, the number of occurrences of each bed type can be set deterministically to be proportional to the overall frequency of each bed type (calculated from the filtered dataset). However, if this option if chosen, bed-types that are less frequent will only be incorporated in generated logs that span a large enough number of beds, unlike in the case of the default stochastic approach.

Thickness values assigned to the beds are governed by thickness data from the filtered dataset and the desired cumulative sand-gravel thickness (in metres) of the modelled log, with a margin of error indicated by an input variable (Table 2). When generating multiple logs simultaneously, a range of cumulative sand-gravel thickness values can be specified from which the algorithm choses a value randomly. For each bed type that is present in the generated artificial log, a lognormal bed-thickness distribution is fitted to the filtered input dataset (Fig. 7). A lognormal distribution is used as a default because it is generally considered as a realistic approximation of the thickness distributions of beds observed in outcrop (e.g., Pantopoulos et al., 2018; Sylvester, 2007). A different type of bed-thickness distribution can be obtained by revising the code. A bed thickness value is assigned to each bed incorporated in the synthetic sedimentary log based on generating random numbers using the mean and standard deviation of the fitted lognormal thickness distribution of the relative bed type (via the 'rlnorm' function). The assignment of bed-thickness values proceeds until the cumulative thickness of the beds falls within the range calculated from the desired sand-gravel thickness and a specified error margin. In cases when the desired sand-gravel thickness cannot be met (e.g., due to imbalance between sand-gravel thickness and the number of beds), the algorithm stops assigning bed thickness values after 100 attempts, and either moves on to the generation of a new log or terminates the process, depending on whether one or multiple logs are being generated. When the script fails to generate a sedimentary log, a warning appears in the console to explain where the code failed.

Transition probabilities for each bed type are used to constrain how

Table 2
Input variables of the synthetic facies-log modelling algorithm (DW-SLG).

	Input variable	Variable name	Description	Type
Analogue dataset filters	Depositional-system grain size	*selected_sys_type*	Dominant grain size of the deep-marine system (sand or gravel-sand dominated) whose element will be represented on the output log. Both options can be selected at the same time.	list
	Architectural-element type	*selected_element*	Architectural-element type (terminal deposit, channel fill or levee) represented on the modelled log. Only one class can be selected.	character/ string
	Global climate	*selected_climate*	Global climate (icehouse, greenhouse) under the modelled element was deposited. Both classes can be selected at the same time.	list
	Age	*selected_period*	Age of the deposits included in the studied dataset (periods of the geological time scale). It allows the exclusion of e.g., Quaternary deposits from the bed-type statistics. By default, the whole geological time scale is selected.	list
Algorithm input variables	Force selected sand-gravel fraction	*try_to_force_NG*	Choose if the script should try to model an element with a certain sand fraction (TRUE or FALSE). If 'FALSE' is selected, the script assign thickness values to mud layers without trying to attain a selected sand fraction value.	logical/ boolean
	Sand-gravel fraction	*selected_NG_value*	Desired sand fraction of the modelled element (0–1). The script uses the mean value calculated from the filtered dataset as default.	numeric
	Allowed sand-gravel fraction margin	*selected_NG_margin*	Allowed discrepancy between desired and modelled sand fraction (0–1). Default value is 0.05.	numeric
	Bed frequency (weighted random/pre set)	*stochastic_bed_frequency*	If TRUE is selected, the bed frequency of the modelled log will be based on weighted random number generation, based on bed-type percentages calculated from the filtered dataset.	logical/ boolean
	Inclusion of sand-mud heterolithic beds	*include_SM_beds*	If FALSE the generated log will not contain sand-mud heterolithic beds.	logical/ boolean
	Inclusion of beds with gravel facies	*include_G_beds*	If FALSE the generated log will not contain beds that have gravel facies (either G, sG or gS type beds).	logical/ boolean
	Total sand-gravel thickness (m)	*selected_sand_thickness*	Cumulative sand thickness of the modelled element in metres. It can take a single value or a range.	numeric
	Allowed tot. sand thickness margin (m)	*selected_sand_thickness_margin*	Allowed discrepancy between desired and modelled cumulative sand thickness in metres. The default value is 0.5 m.	numeric
	Number of beds	*selected_bed_number*	As a default, a value calculated from total sand thickness and mean bed thickness is used. It can be a single value or a range.	numeric
	Start seed	*start_seed*	Seed to control all random number generation used in the script for reproducibility.	Numeric (integer)
	Iteration number	*iteration_number*	Number of logs the user wants to generate.	numeric (integer)

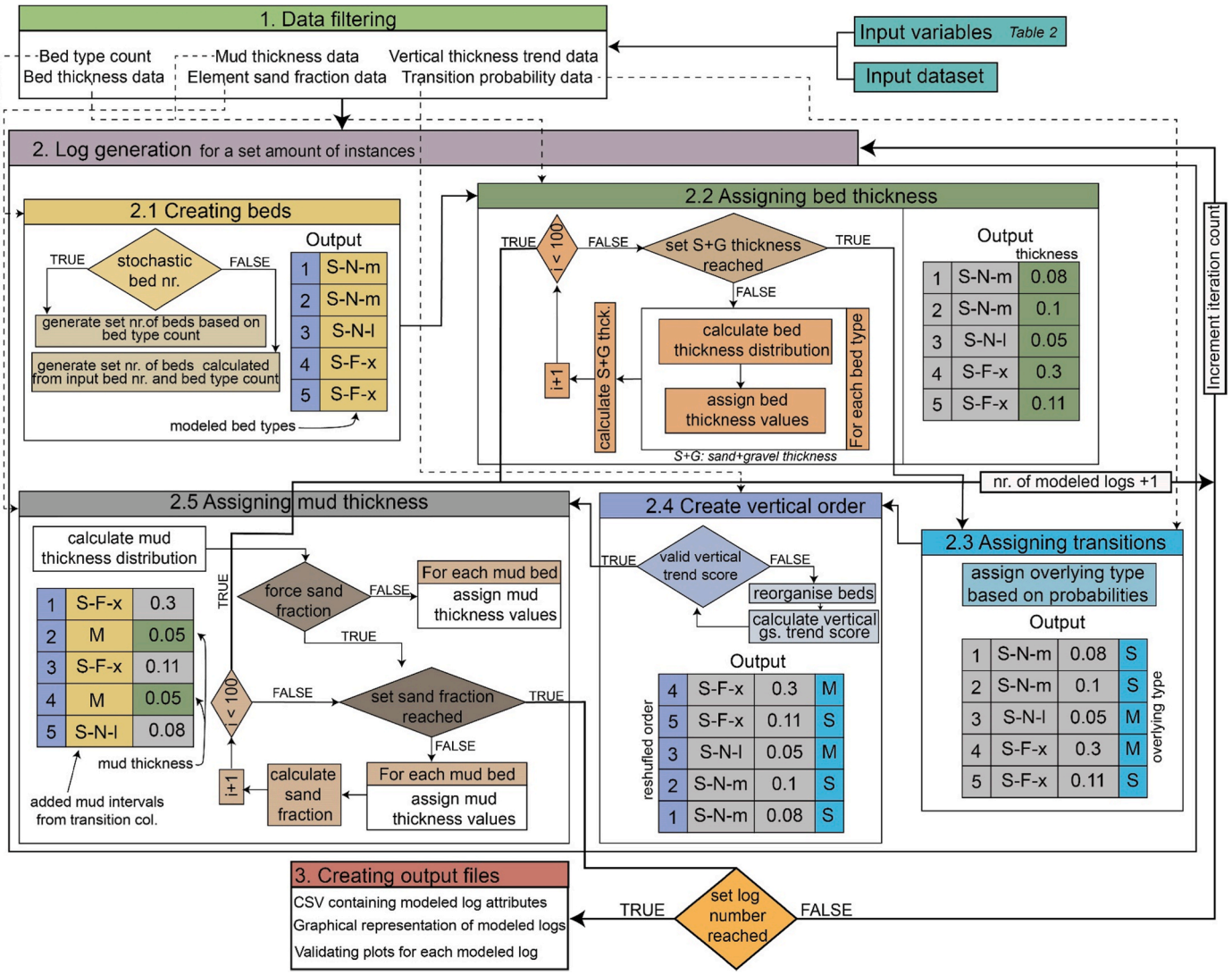

Fig. 7. Workflow of the DW-SLG script. First, an analogue dataset is filtered based on the first set of input variables (including element type, climate, system grain size etc.). The algorithm calculated bed occurences from bed frequency data. As a next step, bed thickness values are assigned for each bed based on fitted lognormal distribution; if the desired cumulative sand thickness cannot be reached the script exits the loop. In the next step, overlying facies types are assigned from vertical transition probabilities. The produced dataframe is then reorganised to reflect a realistic 'vertical thickness trend value'. As the final step, thickness values are assigned to muddy intervals as drawn from a fitted lognormal distribution, with an option to meet a selected sand-gravel fraction. The script then creates text and graphical outputs.

the algorithm produces bed stacking trends, determining whether each output bed is overlain by another sand bed or by mud, using a weighted random number generator (via the 'sample' function), for which the weights are based on the calculated transition probabilities (e.g., Fig. 6B).

As a follow-on step, the modelled sand/gravel beds are rearranged in position through the vertical profile of the log so that any vertical bed thickness trend that may be observed in the selected input analogues is reproduced. To achieve this, firstly, the frequency of upward-thinning or upward-thickening logs in the filtered dataset is sampled by a weighted random number generator to determine whether the modelled log will display thinning-or thickening-upward trends, or no trend (e.g., Fig. 6F). Secondly, a while loop is performed to rearrange each bed entry (row) in the produced dataframe until the calculated 'thickness trend value' (Fig. 6F) falls within the range (minimum to maximum) of values of the filtered analogue dataset (Fig. 7).

The thickness of the muddy intervals in the generated log are assigned using a lognormal distribution fitted to the mud thickness dataset filtered by the input variables (using the 'fitdistr' and 'rlnorm' functions similarly to the bed thickness values) (Fig. 7). If specified by a dedicated Boolean variable (Table 2), the algorithm keeps assigning thickness values to the muddy intervals present in the generated log until a selected sand-gravel fraction is met. If the target sand-gravel fraction cannot be reached within 100 iterations, the algorithm exits the loop (and produces a warning in the console). This may happen if there is a small number of muddy intervals in the generated log, arising from the random sampling of transition probabilities. If instead a specified sand-gravel fraction is not set, the mud thickness values are assigned based on a fitted lognormal distribution without any constraint on the cumulative mud thickness.

4.2. *Modelling outputs*

The R script generates three different outputs saved in a folder named after the modelled architectural-element type:

(i) a CSV file containing the seed number, input variables and properties of each of the generated synthetic sedimentary logs;

these numerical properties include the modelled sand and mud thickness, the element thickness and sand-gravel fraction, and the 'thickness trend value'. By reading this file the reported bedding properties can be utilised as features in machine-learning algorithms for facies-log interpretations.

(ii) Graphical 1D vertical sections of the generated log(s) in PDF format, editable using vector-based graphical software (Fig. 8).

(iii) Charted summary information on sand-gravel fraction, mud thickness, vertical thickness trends and bed thickness calculated on the dataset filtered by input variables. These plots also show the same values for the generated logs for comparison against the filtered analogue dataset that underpins them (Fig. 9).

The generation of graphical outputs increases the run time, but is only optional. The name of each output file contains the seed number, the element type, the type of the output file and a timestamp indicating the time of creation.

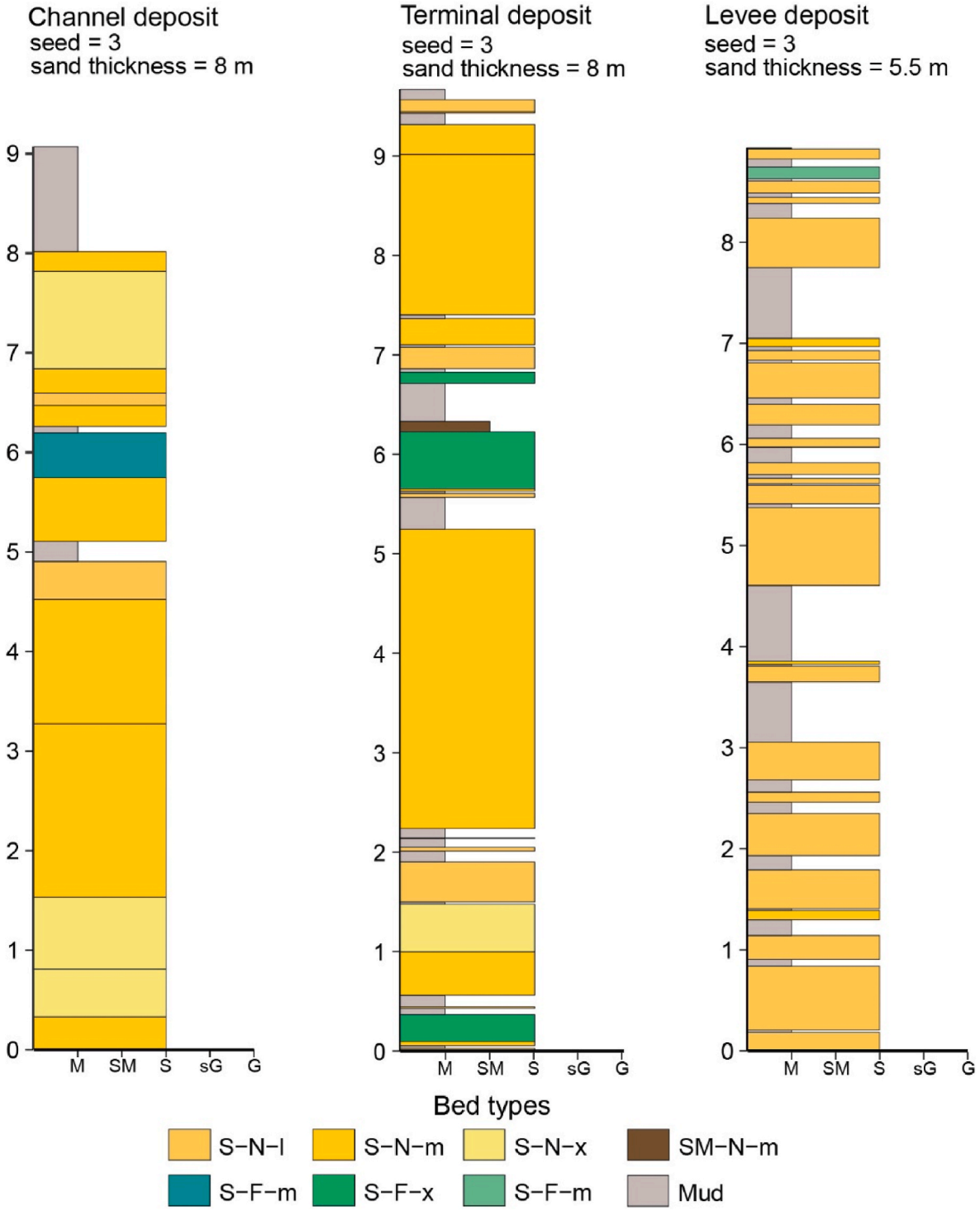

Fig. 8. Example outputs from the DW-SLG script. 1D depiction of channel-fill, terminal deposit and levee deposits of comparable thickness.

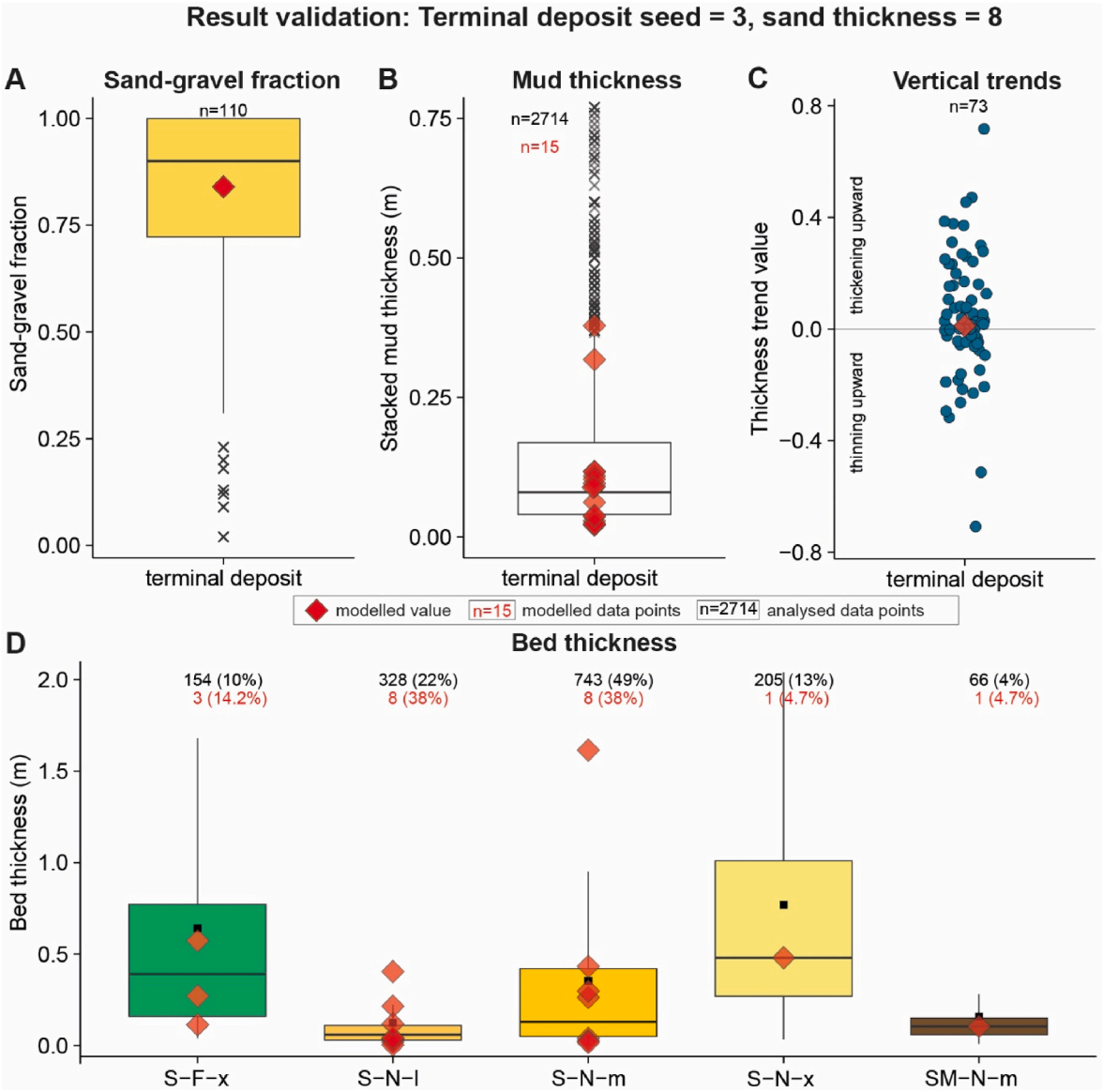

Fig. 9. Graphical outputs on the comparison of synthetic 1D sedimentary logs generated using the proposed algorithm with the underlying data from the sedimentological database of geological analogues. The box plots show distributions in sand fraction (A), mud thickness (B), vertical thickness trends (C) and sand bed thickness (D) of terminal deposits of sandy systems in the database, compared against corresponding values (red squares) for a modelled sedimentary log depicting a terminal deposit represented in Fig. 8. (For interpretation of the references to colour in this figure legend, the reader is referred to the Web version of this article.)

5. Discussion and conclusions

Deep-water architectural elements are composed of beds whose facies properties, act as records of sedimentary processes linked to tectonic, climatic, and sea-level controls, and, have a major impact on subsurface reservoir characteristics. This study has addressed the need to develop a generic bed classification scheme and method that can be utilised to bring together data on bedding properties across different case studies. In turn, this makes it easier to apply geological analogues in subsurface interpretation workflows and will facilitate comparisons across deep-water sedimentary successions.

By utilising a large database of global scope and based on the integration of many data sources, it is ensured that the proposed deep-water bed-type scheme can be applied broadly to sedimentological datasets. Meanwhile, the statistical characterisation of deep-water architectural elements presented herein supports the use of the proposed scheme in contexts of subsurface interpretations and predictions. The proposed sedimentary-bed classification scheme feeds into a novel stochastic algorithm for the creation of 1D synthetic sedimentary logs for specific architectural-element types, which can be utilised as machine-learning training data for automating sedimentological interpretations of sedimentary logs. This is particularly applicable to the process of labelling facies logs in subsurface successions, a process that may itself be based on the application of machine-learning approaches (e.g., Hall, 2016; Bressan et al., 2020) and that determines categorisation of borehole data at the architectural-element scale for conditioning geocellular facies models. Importantly, the proposed approach allows generation of large training datasets based on data from outcrop analogues, in which facies and architectures are seen. It is hoped that such training dataset will enable automatic predictions of subsurface sedimentary architectures (cf. Colombera and Budai, 2025).

Current limitations of the sedimentary-log modelling algorithm could be addressed in the future with the inclusion of the option to model multiple, vertically superimposed elements at the same time. Currently, transition probabilities between beds of different types are not considered in the process of vertical ordering; this could also be

addressed. Furthermore, vertical trends of the modelled logs could be improved by the analysis and application of thickness relationship between superimposed beds.

The illustrated workflow can be generalised to the characterisation of other clastic and carbonate depositional systems, and therefore it holds promise as a way to digest and apply large sedimentological datasets for both fundamental and applied investigations.

CRediT authorship contribution statement

Soma Budai: Writing – review & editing, Writing – original draft, Visualization, Software, Formal analysis, Data curation, Conceptualization. **Luca Colombera:** Writing – review & editing, Methodology, Conceptualization. **Adam McArthur:** Writing – review & editing, Methodology, Funding acquisition, Conceptualization. **Marco Patacci:** Writing – review & editing, Methodology, Conceptualization.

Code availability section

Name of the code/library: DW-BC and DW-SLG
Contact: soma.budai@unipv.it
Program language: R
Software required: R version 4.4.1

The source codes along with explanatory ".md" files, dummy datasets and MIT open access licence are available in the following GitHub repository: https://github.com/somabudai/deep_water_bed_types

Declaration of competing interest

The authors declare that they have no known competing financial interests or personal relationships that could have appeared to influence the work reported in this paper.

Acknowledgements

We thank the sponsors of the Turbidites Research Group (AkerBP, CNOOC, ConocoPhillips, ENI, Harbour Energy, Murphy, OMV, Oxy, and PetroChina) for their financial support to this work. We also thank two anonymous reviewers for their constructive comments and suggestions.

Data availability

Data will be made available on request.

References

Baas, J.H., Tracey, N.D., Peakall, J., 2021. Sole marks reveal deep-marine depositional process and environment: implications for flow transformation and hybrid-event-bed models. J. Sediment. Res. 91, 986–1009. https://doi.org/10.2110/jsr.2020.104.

Baker, M.L., Baas, J.H., 2020. Mixed sand–mud bedforms produced by transient turbulent flows in the fringe of submarine fans: indicators of flow transformation. Sedimentology 67, 2645–2671. https://doi.org/10.1111/sed.12714.

Barton, M.D., Craig, P., Prather, B.E., Copus, J., 2007a. Facies architecture of channel-levee deposits, lago nordenskjold and laguna mellizas sur, cerro toro formation, Chile. In: Nilsen, T.H., Shew, R.D., Steffens, G.S., Studlick, J.R.J. (Eds.), Atlas of Deep-Water Outcrops. AAPG Studies in Geology, pp. 157–161. https://doi.org/10.1306/1240928St563289.

Barton, M.D., O`Byrne, C.J., Steffens, Gary S., Pirmez, C., Buergisser, H., 2007b. Architecture of an aggradational deep-water channel complex: channel complex 2, isaac formation, windermere supergroup, British columbia, Canada. In: Nilsen, T.H., Shew, R.D., Steffens, G.S., Studlick, J.R.J. (Eds.), Atlas of Deep-Water Outcrops, AAPG Studies in Geology, pp. 106–110. https://doi.org/10.1306/1240915St563289.

Bell, D., Kane, I.A., Pontén, A.S.M., Flint, S.S., Hodgson, D.M., Barrett, B.J., 2018. Spatial variability in depositional reservoir quality of deep-water channel-fill and lobe deposits. Mar. Petrol. Geol. 98, 97–115. https://doi.org/10.1016/j.marpetgeo.2018.07.023.

Bouma, A.H., 1962. Sedimentology of some flysch deposits. A Graphic Approach to Facies Interpretation. Elsevier, Amsterdam.

Bourget, J., Zaragosi, S., Mulder, T., Schneider, J.L., Garlan, T., Van Toer, A., Mas, V., Ellouz-Zimmermann, N., 2010. Hyperpycnal-fed turbidite lobe architecture and recent sedimentary processes: a case study from the Al Batha turbidite system, Oman margin. Sediment. Geol. 229, 144–159. https://doi.org/10.1016/j.sedgeo.2009.03.009.

Brandes, C., Struss, I., Vandré, C., Winsemann, J., 2007. Architecture of proximal midfan levee deposits, punta farallones La flor, Nicaragua. In: Nilsen, T.H., Shew, R.D., Steffens, G.S., Studlick, J.R.J. (Eds.), Atlas of Deep-Water Outcrops. AAPG Studies in Geology, pp. 271–273. https://doi.org/10.1306/1240954St563303.

Bressan, T.S., Kehl de Souza, M., Girelli, T.J., Junior, F.C., 2020. Evaluation of machine learning methods for lithology classification using geophysical data. Comput. Geosci. 139. https://doi.org/10.1016/j.cageo.2020.104475.

Brunt, R.L., 2003. Vertical transitions in turbidite facies and sedimentary architecture: insights from the Grès du Champsaur, SE France, and from laboratory experiments. The University of Leeds, Leeds.

Callow, R.H.T., McIlroy, D., Kneller, B., Dykstra, M., 2013. Ichnology of late cretaceous turbidites from the rosario formation, baja California, Mexico. Ichnos 20, 1–14. https://doi.org/10.1080/10420940.2012.734763.

Campion, K.M., Sprague, A.R., Sullivan, M.D., 2007. Architecture and lithofacies of the miocene capistrano formation, san clemente state beach, California, USA. In: Nilsen, T.H., Shew, R.D., Steffens, G.S., Studlick, J.R.J. (Eds.), Atlas of Deep-Water Outcrops. AAPG Studies in Geology, pp. 395–400 https://doi.org/10.130611240982St56632.

Celis, S.A., García-García, F., Rodríguez-Tovar, F.J., Giraldo-Villegas, C.A., Pardo-Trujillo, A., 2024. Coarse-grained submarine channels: from confined to unconfined flows in the Colombian Caribbean (late Eocene). Sediment. Geol. 459. https://doi.org/10.1016/j.sedgeo.2023.106550.

Colombera, L., Budai, S., 2025. Identification of shallow-water clastic parasequences in borehole data using machine learning trained on geologic analogs. In: Feldman, H., Ainsworth, R.B., Colombera, L., Caldwell, R.L. (Eds.), SEPM Special Publication, Are Parasequences Still Relevant? (in press).

Cronin, B.T., Jones, M.A., 2018. Facies classification and facies association of deep-water depositional systems: application to the prediction of slope and fan architecture in the upper jurassic THELMA field area, south viking graben, north sea. AAPG Memoir 115, 339–386. https://doi.org/10.1306/13652187M1153311.

Cullis, S., Patacci, M., Colombera, L., Bührig, L., McCaffrey, W.D., 2019. A database solution for the quantitative characterisation and comparison of deep-marine siliciclastic depositional systems. Mar. Petrol. Geol. 102, 321–339. https://doi.org/10.1016/j.marpetgeo.2018.12.023.

Danukalova, M.K., Kuzmichev, A.B., Sennikov, N.V., Tolmacheva, T.Y., 2020. Ordovician turbidites and black shales of bennett island (De long islands, Russian arctic), and their significance for arctic correlations and palaeogeography. Geol. Mag. 157, 1207–1237. https://doi.org/10.1017/S0016756819001341.

De Ruig, M.J., Hubbard, S.M., 2006. Seismic facies and reservoir characteristics of a deep-marine channel belt in the Molasse foreland basin, Puchkirchen Formation, Austria. AAPG (Am. Assoc. Pet. Geol.) Bull. 90, 735–752. https://doi.org/10.1306/10210505018.

Deptuck, M.E., Piper, D.J.W., Savoye, B., Gervais, A., 2008. Dimensions and architecture of late Pleistocene submarine lobes off the northern margin of East Corsica. Sedimentology 55, 869–898. https://doi.org/10.1111/j.1365-3091.2007.00926.x.

Dykstra, M., Kneller, B., 2007. Canyon sand fernando, Mexico: a deep-water, channel-levee complex exhibiting evolution from submarine canyon-confined to unconfined. In: Nilsen, T.H., Shew, R.D., Steffens, G.S., Studlick, J.R.J. (Eds.), Atlas of Deep-Water Outcrops. AAPG Studies in Geology, pp. 226–229. https://doi.org/10.1306/1240943St563284.

Felletti, F., 2002. Complex bedding geometries and facies associations of the turbiditic fill of a confined basin in a transpressive setting (Castagnola Fm., Tertiary Piedmont Basin, NW Italy). Sedimentology 49, 645–667. https://doi.org/10.1046/j.1365-3091.2002.00467.x.

Felletti, F., 2004. Statistical modelling and validation of correlation in turbidites: an example from the tertiary piedmont basin (castagnola Fm., northern Italy). Mar. Petrol. Geol. 21, 23–39. https://doi.org/10.1016/j.marpetgeo.2003.11.006.

Felletti, F., Bersezio, R., 2010. Validation of Hurst statistics: a predictive tool to discriminate turbiditic sub-environments in a confined basin. Pet. Geosci. 16, 401–412. https://doi.org/10.1144/1354-079309-005.

Figueiredo, J.J.P., Hodgson, D.M., Flint, S.S., Kavanagh, J.P., 2010. Depositional environments and sequence stratigraphy of an exhumed permian mudstone-dominated submarine slope succession, Karoo Basin, South Africa. J. Sediment. Res. 80, 97–118. https://doi.org/10.2110/jsr.2010.002.

Folk, RobertL., 1980. Petrologie of Sedimentary Rocks. Hemphill Publishing Company, Austin, p. 181.

Fryer, R.C., Jobe, Z.R., 2019. Quantification of the bed-scale architecture of submarine depositional environments. Depositional Record 5, 192–211. https://doi.org/10.1002/dep2.70.

Geehan, G., Underwood, J., 1993. The use of length distributions in geological modelling. In: Flint, S.S., Bryant, I.D. (Eds.), The Geological Modelling of Hydrocarbon Reservoirs and Outcrop Analogues, vol. 15. IAS Special Publication, pp. 205–212.

Gervais, A., Savoye, B., Mulder, T., Gonthier, E., 2006. Sandy modern turbidite lobes: a new insight from high resolution seismic data. Mar. Petrol. Geol. 23, 485–502. https://doi.org/10.1016/j.marpetgeo.2005.10.006.

Ghibaudo, G., 1992. Subaqueous sediment gravity flow deposits: practical criteria for their field description and classification. Sedimentology 39, 423–545.

Hall, B., 2016. Facies classification using machine learning. Lead. Edge 35, 906–909.

Halotel, J., Demyanov, V., Gardiner, A., 2020. Value of geologically derived features in machine learning facies classification. Math. Geosci. 52, 5–29. https://doi.org/10.1007/s11004-019-09838-0.

Hofstra, M., Hodgson, D.M., Peakall, J., Flint, S.S., 2015. Giant scour-fills in ancient channel-lobe transition zones: formative processes and depositional architecture. Sediment. Geol. 329, 98–114. https://doi.org/10.1016/j.sedgeo.2015.09.004.

Jackson, C.A.L., Larsen, E., Hanslien, S., Tjemsland, A.E., 2011. Controls on synrift turbidite deposition on the hanging wall of the South Viking Graben, North Sea rift system, offshore Norway. Am. Assoc. Petrol. Geol. Bull. 95, 1557–1587. https://doi.org/10.1306/01031110037.

Jobe, Z., Seckinger, C., Martin, T., Kus, K., Pettinga, L., 2024. Lateral heterogeneity of basin-plain turbidites of the Cloridorme Formation, Quebec, Canada: implications for horizontal well prediction. Depositional Record. https://doi.org/10.1002/dep2.278.

Kane, I.A., Kneller, B.C., Dykstra, M., Kassem, A., McCaffrey, W.D., 2007. Anatomy of a submarine channel-levee: an example from upper cretaceous slope sediments, rosario formation, baja California, Mexico. Mar. Petrol. Geol. 24, 540–563. https://doi.org/10.1016/j.marpetgeo.2007.01.003.

Kane, I.A., Dykstra, M.L., Kneller, B.C., Tremblay, S., McCaffrey, W.D., 2009. Architecture of a coarse-grained channel-levée system: the rosario formation, baja California, Mexico. Sedimentology 56, 2207–2234. https://doi.org/10.1111/j.1365-3091.2009.01077.x.

Kane, I.A., Pontén, A.S.M., Vangdal, B., Eggenhuisen, J.T., Hodgson, D.M., Spychala, Y. T., 2017. The stratigraphic record and processes of turbidity current transformation across deep-marine lobes. Sedimentology 64, 1236–1273. https://doi.org/10.1111/sed.12346.

Łapcik, P., 2017. Facies heterogeneity of a deep-sea depositional Lobe complex: case study from the Słonne section of skole nappe, Polish outer carpathians. Ann. Soc. Geol. Pol. 87, 301–324. https://doi.org/10.14241/asgp.2017.017.

Łapcik, P., 2024. Evolution of a turbidite system in a narrow basin setting: the ropianka Fm (Campanian–Paleocene) in the skole nappe of the polish carpathians. Ann. Soc. Geol. Pol. https://doi.org/10.14241/asgp.2024.03.

Larsen, P.-H., Escher, J.C., 1991. A stratigraphic section through the silurian turbidite sequence (peary land group) in northern nyeboe land, north Greenland. Rapp. - Grnl. Geol. Undersgelse 151.

Li, P., Kneller, B.C., Hansen, L., Kane, I.A., 2016. The classical turbidite outcrop at San Clemente, California revisited: an example of sandy submarine channels with asymmetric facies architecture. Sediment. Geol. 346, 1–16. https://doi.org/10.1016/j.sedgeo.2016.10.001.

Lowe, D.R., 1982. Sediment Gravity Flows : II . Depositional models with special reference to the deposits of high-density turbidity currents. J. Sediment. Petrol. 52, 279–297. https://doi.org/10.1306/212F7F31-2B24-11D7-8648000102C1865D.

Martin, T., Meyer, R., Jobe, Z., 2021. Centimeter-scale lithology and facies prediction in cored wells using machine learning. Front. Earth Sci. 9. https://doi.org/10.3389/feart.2021.659611.

Martin, T., Tadla, J., Jobe, Z., 2022. Digitalization of legacy datasets and machine learning regression yields insights for reservoir property prediction and submarine-fan evolution: a subsurface example from the lewis shale, Wyoming. Sediment. Rec. 20. https://doi.org/10.2110/001c.36638.

McKie, T., Rose, P.T.S., Hartley, A.J., Jones, D.W., Armstrong, T.L., 2015. Tertiary Deep-Marine Reservoirs of the North Sea Region: an Introduction. Geological Society Special Publication. Geological Society of, London, pp. 1–16. https://doi.org/10.1144/SP403.12.

Morris, E.A., Hodgson, D.M., Brunt, R.L., Flint, S.S., 2014a. Origin, evolution and anatomy of silt-prone submarine external levées. Sedimentology 61, 1734–1763. https://doi.org/10.1111/sed.12114.

Morris, E.A., Hodgson, D.M., Flint, S.S., Brunt, R.L., Butterworth, P.J., Verhaeghe, J., 2014b. Sedimentology, stratigraphic architecture, and depositional context of submarine frontal-lobe complexes. J. Sediment. Res. 84, 763–780. https://doi.org/10.2110/jsr.2014.61.

Mulder, T., Alexander, J., 2001. The physical character of subaqueous sedimentary density flow and their deposits. Sedimentology 48, 269–299. https://doi.org/10.1046/j.1365-3091.2001.00360.x.

Müller, K., Ooms, J., James, D., DebRoy, S., Wickham, H., Horner, J., 2024. RMariaDB: database interface and MariaDB driver. https://rmariadb.r-dbi.org.

Mutti, E., 1992. Turbidite sandstones. Agip, Instituto di Geologia, Univerità di Parma, San Donato Milanese, p. 275.

Mutti, E., Normark, W.R., 1987. Comparing examples of modern and ancient turbidite systems: problems and concepts. In: Legett, J.K., Zuffa, G.G. (Eds.), Marine Clastic Sedimentology. Graham and Trotman, London, pp. 1–138. https://doi.org/10.1007/978-94-009-3241-8.

Mutti, E., Normark, W.R., 1991. An integrated approach to the study of turbidite systems. In: Weimer, P., Link, H. (Eds.), Seismic Facies and Sedimentary Processes of Submarine Fans and Turbidite. Springer-Verlag, New York, pp. 75–106.

Navarro, L., Khan, Z.A., Arnott, R.W.C., 2007. Architecture of a deep-water channel-levee complex: channel 3, castle creek south, isaac formation, windermere supergroup, British columbia, Canada. In: Nilsen, T.H., Shew, R.D., Steffens, G.S., Studlick, J.R.J. (Eds.), Atlas of Deep-Water Outcrops. AAPG Studies in Geology, pp. 93–96. https://doi.org/10.1306/1240911St563288.

Ningthoujam, J., Wearmouth, C., Arnott, R.W.C., 2022. Stratal characteristic and depositional origin of two-part (Mud-poor overlain by mud-rich) and associated deep-water strata: components in a lateral depositional continuum related to particle settling in negligibly sheared mud-rich suspensions. J. Sediment. Res. 92, 503–529. https://doi.org/10.2110/jsr.2021.053.

Normark, W.R., 1970. Growth patterns of deep-sea fans. Am. Assoc. Petrol. Geol. Bull. 54, 2170–2195. https://doi.org/10.1306/5D25CC79-16C1-11D7-8645000102C1865D.

O'Byrne, C.J., Barton, M.D., Prather, B., Pirmez, C., Sylvester, Z., Commins, D., Coffa, A., 2007. Deep-water channel-complex architecture, popo fault block, brushy canyon formation, Texas, USA-Part 1: stratal framework. In: Nilsen, T.H., Shew, R.D., Steffens, G.S., Studlick, J.R.J. (Eds.), Atlas of Deep-Water Outcrops. AAPG Studies in Geology, pp. 457–462. https://doi.org/10.1306/1240995St563290.

Pantopoulos, G., Kneller, B.C., McArthur, A.D., Courivaud, S., Grings, A.E., Kuchle, J., 2018. Turbidite bed thickness statistics of architectural elements in a deep-marine confined mini-basin setting: examples from the Grès d'Annot Formation, SE France. Mar. Petrol. Geol. 95, 16–29. https://doi.org/10.1016/j.marpetgeo.2018.04.008.

Pichevin, L., Mulder, T., Savoye, B., Gervais, A., Cremer, M., Piper, D.J.W., 2003. The Golo submarine turbidite system (east Corsica margin): morphology and processes of terrace formation from high-resolution seismic reflection profiles. Geo Mar. Lett. 23, 117–124. https://doi.org/10.1007/s00367-003-0131-4.

Pickering, K.T., Stow, D., Watson, M., Hiscott, R., 1986. Deep-water faces, processes and models: a review and classification scheme for modern and ancient sediments. Earth Sci. Rev. 23, 75–174.

Pickering, K.T., Clark, J.D., Smith, R.D.A., Hiscott, R.N., Lucchi, F.R., Kenyon, N.H., 1995. Architectural element analysis of turbidite systems, and selected topical problems for sand-prone deep-water systems. In: Pickering, K.T., Clark, J.D., Smith, R.D.A., Hiscott, R.N., Lucchi, R.F., Kenyon, N.H. (Eds.), Atlas OfDeep Water Environments: Architectural Styles in Turbidite Systems. Chapman & Hall, London, pp. 1–11.

Pickering, K.T., Hilton, V.C., 1998. Turbidite Systems of Southeast France. Vallis Press, London.

Prélat, A., Hodgson, D.M., Flint, S.S., 2009. Evolution, architecture and hierarchy of distributary deep-water deposits: a high-resolution outcrop investigation from the Permian Karoo Basin, South Africa. Sedimentology 56, 2132–2154. https://doi.org/10.1111/j.1365-3091.2009.01073.x.

Pyles, D.R., 2007a. Architectural elements in a ponded submarine fan, ross sandstone, Ireland. In: Nilsen, T.H., Shew, R.D., Steffens, G.S., Studlick, J.R.J. (Eds.), Atlas of Deep-Water Outcrops. AAPG Studies in Geology, pp. 206–209. https://doi.org/10.1306/1240939St562471.

Pyles, D.R., 2007b. Architectural elements in a ponded submarine fan, carboniferous ross sandstone, western Ireland. In: Nilsen, T.H., Shew, R.D., Steffens, G.S., Studlick, J.R. J. (Eds.), Atlas of Deep-Water Outcrops. AAPG Studies in Geology, pp. 1–19. https://doi.org/10.1306/12401017St562471.

Pyles, D.R., Jennette, D.C., Tomasso, M., Beaubouef, R.T., Rossen, C., 2010. Concepts learned from a 3d outcrop of a sinuous slope channel complex: beacon channel complex, brushy canyon formation, West Texas. U.S.A. J. Sedimentary Res. 80, 67–96. https://doi.org/10.2110/jsr.2010.009.

R Core Team, 2021. R: A Language and Environment for Statistical Computing. R Foundation for Statistical Computing, Vienna, Austria. URL. https://www.R-project.org/.

Staňová, S., Soták, J., Hudec, N., 2009. Markov chain analysis of turbiditic facies and flow dynamics (Magura Zone, Outer Western Carpathians, NW Slovakia). Geol. Carpathica 60, 295–305. https://doi.org/10.2478/v10096-009-0021-4.

Stright, L., Stewart, J., Campion, K., Graham, S., 2014. Geologic and seismic modeling of a coarse-grained deep-water channel reservoir analog (Black's Beach, La Jolla, California). Am. Assoc. Petrol. Geol. Bull. 98, 695–728. https://doi.org/10.1306/09121312211.

Struss, I., Brandes, P., Kischkies, M., Winsemann, J., 2007. Channel geometries and internal deformaiton patterns of the playa las tablas Channel-levee system, Nicaragua. In: Nilsen, T.H., Shew, R.D., Steffens, G.S., Studlick, J.R.J. (Eds.), Atlas of Deep-Water Outcrops. AAPG Studies in Geology, pp. 265–267 https://doi.org/10.130611240952St563303.

Sylvester, Z., 2007. Turbidite bed thickness distributions: methods and pitfalls of analysis and modelling. Sedimentology 54, 847–870. https://doi.org/10.1111/j.1365-3091.2007.00863.x.

Talling, P.J., Masson, D.G., Sumner, E.J., Malgesini, G., 2012. Subaqueous sediment density flows: depositional processes and deposit types. Sedimentology 59, 1937–2003. https://doi.org/10.1111/j.1365-3091.2012.01353.x.

Tinterri, R., Piazza, A., 2019. Turbidites facies response to the morphological confinement of a foredeep (Cervarola Sandstones Formation, Miocene, northern Apennines, Italy). Sedimentology 66, 636–674. https://doi.org/10.1111/sed.12501.

Tőkés, L., Patacci, M., 2018. Quantifying tabularity of turbidite beds and its relationship to the inferred degree of basin confinement. Mar. Petrol. Geol. 97, 659–671. https://doi.org/10.1016/j.marpetgeo.2018.06.012.

Trexler, J.H., Cashman, P.H., 1997. A southern antler foredeep submarine fan: the mississippian eleana formation, Nevada test site. J. Sediment. Res. 67, 1044–1059. https://doi.org/10.1306/d42686c1-2b26-11d7-8648000102c1865d.

Wang, Z., Fan, R., Zong, R., Gong, Y., 2021. Composition and spatiotemporal evolution of the mixed turbidite-contourite systems from the Middle Ordovician, in western margin of the North China Craton. Sediment. Geol. 421. https://doi.org/10.1016/j.sedgeo.2021.105943.

Wickham, H., 2016. ggplot2: Elegant Graphics for Data Analysis. Springer-Verlag, New York.

Wickham, H., François, R., Henry, L., Müller, K., Vaughan, D., 2023. Dplyr: a grammar of data manipulation. R package version 1.1.4. https://dplyr.tidyverse.org.

Yang, S.Y., Kim, J.W., 2014. Pliocene basin-floor fan sedimentation in the Bay of Bengal (offshore northwest Myanmar). Mar. Petrol. Geol. 49, 45–58. https://doi.org/10.1016/j.marpetgeo.2013.09.007.